

## Electronic Supplementary Information

### Exploring the electronic structure and speciation of aqueous and colloidal Pu with high energy resolution XANES and computations

Tonya Vitova,\* Ivan Pidchenko, David Fellhauer, Tim Pruessmann, Sebastian Bahl, Kathy Dardenne, Tadahiro Yokosawa, Bernd Schimmelpfennig, Marcus Altmaier, Melissa Denecke, Jörg Rothe and Horst Geckeis

Institute for Nuclear Waste Disposal (INE), Karlsruhe Institute of Technology, P.O. 3640, D-76021 Karlsruhe, Germany.

**24<sup>th</sup> May 2019 – Note added after first publication:** This Supplementary Information file replaces that originally published on 29<sup>th</sup> October 2018. On page S5, the emission energy value for the Pu M $\alpha$  line was incorrectly written as 3339 eV. This has been corrected to 3351 eV. Reference 7 was also added in the caption to Fig. S10.

## Experimental section

### Figures

**Fig. S1.** Vis-NIR spectra of Pu(III)<sub>aq</sub> (a), Pu(IV)<sub>aq</sub> (b, bottom), Pu(IV)<sub>col</sub> (b, top), Pu(V)<sub>aq</sub> (c) and Pu(VI)<sub>aq</sub> (d) before (colored curve) and after (black dashed curve) the Pu L<sub>3</sub> edge HR-XANES & XAFS experiments.

**Fig. S2.** Vis-NIR spectra of Pu(IV)<sub>col</sub> samples measured before or after HR-XANES/XAFS/TEM experiments (cf. Table S1).

**Fig. S3.** Particle size distribution of colloidal Pu derived from the TEM image (cf. Fig. S4).

**Fig. S4.** HR-TEM image, STEM-EDX and EELS spectra of nanometer-sized PuO<sub>2</sub> colloids. The EELS spectrum shows the O<sub>4,5</sub> edge of Pu.

**Fig. S5.** 3d view of the inert gas cell used for the L<sub>3</sub> and M<sub>5</sub> edge experiments (top); 3d view (top) and a photograph (bottom) of the liquid cells used for the M<sub>5</sub> edge experiments. A photograph of the aqueous and colloidal Pu samples prepared for the Pu L<sub>3</sub> edge HR-XANES/XAFS experiments (bottom right).

**Fig. S6.** Magnitude of Fourier transformed EXAFS spectra (coloured rhombs) and their best fits (dash dot line) for Pu(III)<sub>aq</sub>, Pu(IV)<sub>aq</sub>, Pu(IV)<sub>col</sub>, Pu(V)<sub>aq</sub> and Pu(VI)<sub>aq</sub>. The arrow indicates Pu-Pu coordination peak in Pu(IV)<sub>col</sub>.

**Fig. S7.** EXAFS spectra in k and back transformed q range and their best fits for the Pu(III)<sub>aq</sub>, Pu(IV)<sub>aq</sub>, Pu(IV)<sub>col</sub>, Pu(V)<sub>aq</sub> and Pu(VI)<sub>aq</sub>.

**Fig. S8.** The unit cell of PuO<sub>2</sub> (ICSD 55456), The lattice constant a = 5.398 Å is given.

**Fig. S9.** The experimental Pu L<sub>3</sub> HR-XANES spectrum for Pu(VI)<sub>aq</sub> modeled with three Voigt profiles and one arctan function.

**Fig. S10.** U M<sub>4</sub> HR-XANES spectra of UO<sub>2</sub> and U<sub>4</sub>O<sub>9</sub> reported in references 1 and 7.

**Fig. S11.** Pu L<sub>3</sub> HR-XANES: experiment and calculations with the FEFF9.5 code and Pu d- and f-DOS for Pu(III)<sub>aq</sub>.

### Tables

**Table S1.** Experimental plan for the aqueous and colloidal Pu samples. Vis-NIR spectra are measured before and after the synchrotron/TEM experiments (cf. footnotes); The equilibration time for the colloids is given relative to the preparation of the colloidal sample for the L<sub>3</sub> edge experiments; The pH is also indicated in the last column.

**Table S2.** EXAFS fit results: SP – scattering path, N – coordination number, R – bond distance,  $\sigma^2$  – Debye-Waller factor,  $\Delta E_0$  – energy shift of the ionization potential,  $S_0^2$  – amplitude reduction factor and r – goodness of fit parameter. N\* and R\*- coordination numbers and average interatomic distances derived from optimized

structures with TURBOMOLE (Pu(IV)aq, Pu(V)aq, Pu(VI)aq) or PuO<sub>2</sub> ICSD 55456 (Pu(IV)col);\*\* Published coordination number and interatomic distances.

**Table S3.** Spectral feature, Height, Position and Full width at half maximum (FWHM) parameters of the PV functions used to model the Pu L<sub>3</sub> HR-XANES spectrum and an arctangent used to model the edge jump; the Gauss part (Gauss part  $\alpha$ ) and the area of the PV profiles (Area PV); the residual between experimental data and best fit (Residual %);<sup>f</sup> denotes that the parameter is fixed during the fit.

**Table S4.** Input parameters used in the feff.inp files.

## Experimental section

**Table S1.** Experimental plan for the aqueous and colloidal Pu samples. Vis-NIR spectra are measured before and after the synchrotron/TEM experiments (cf. footnotes); The equilibration time for the colloids is given relative to the preparation of the colloidal sample for the L<sub>3</sub> edge experiments; The pH is also indicated in the last column.

		Pu(III)aq	Pu(IV)aq	Pu(V)aq	Pu(VI)aq	Pu(IV)col	Equilibration time for the colloids, pH
1	Pu L <sub>3</sub> HR-XANES & XAFS	x	x	x	x	x	+10 days, pH 0
2	Pu M <sub>5</sub> XANES	x	x		x	x*	+ 9 months, pH 1
3	TEM					x**	+ 9 months, pH 2
4	Pu M <sub>5</sub> HR-XANES	x			x		
5	Pu M <sub>5</sub> HR-XANES		x			x***	+22 months, pH 0.3

\*Only the Vis-NIR spectra are shown in Figure S2; the Pu M<sub>5</sub> XANES spectrum is not shown;

\*\* The sample is dried on a TEM grid therefore Vis-NIR is not possible after the TEM measurements (cf. TEM section);

\*\*\* Due to the small amount of sample Vis-NIR was measured only before the synchrotron experiments.

## Preparation of Pu(III)aq-Pu(VI)aq and Pu(IV)col

### Pu L<sub>3</sub> HR-XANES and XAFS: Pu(III)aq-Pu(VI)aq and Pu(IV)col

Pure solutions of Pu (0.01-0.03 M Pu(III), Pu(IV), Pu(V), and Pu(VI)) in 1 M HClO<sub>4</sub>/NaClO<sub>4</sub> media were prepared electrochemically in an inert gas glove box starting from a purified colloid free 0.05 M Pu(III/IV) stock solution in 1 M HClO<sub>4</sub>. The successive electrochemical steps are briefly outlined: an aliquot of the Pu(III/IV) stock solution was quantitatively reduced to Pu(III) at a potential of E = -400 mV (E values are measured versus Ag/AgCl + 3 M NaCl). Rapid oxidation of Pu(III) at E = 900 mV yielded a solution of 91% Pu(IV)<sub>aq</sub> + 9% Pu(VI)<sub>aq</sub> (L<sub>3</sub> edge). Subsequent oxidation at E = 1900 mV led to pure Pu(VI) solutions. An aliquot of the latter was neutralized with 1 M NaOH (final pH ~ 4) and carefully reduced to pure Pu(V) by applying a potential of E = 600 mV. For all spectroscopy measurements, a 350  $\mu$ l aliquot was taken from each fraction before the following electrochemical step. Vis-NIR spectra of the samples were recorded before and after the synchrotron based measurements; 100% purity was achieved for the Pu(III) and Pu(VI) solutions.

0.004 M colloidal Pu(IV) solution in 1 M HClO<sub>4</sub> (96% Pu(IV)<sub>col</sub> + 4% Pu(IV)<sub>aq</sub>) was obtained by separation of Pu(IV) colloids from a supersaturated Pu(IV) solution using a 10 kD (2 nm) ultrafiltration step, washing with H<sub>2</sub>O and 1 M HClO<sub>4</sub> (pH 0), and resuspension in 500  $\mu$ L of 1 M HClO<sub>4</sub>.

No significant changes in the oxidation states after the synchrotron experiments were detected: the spectra show insignificant variations of about 2% (Figure S1, S2). One exception is Pu(V)aq as 7% of the initial Pu(V)aq has disproportionated to [6% Pu(IV)col + 1% Pu(VI)aq]. Before the HR-XANES experiments 96% Pu(V) and 0.4% Pu(VI) were found in the sample.

### Pu M<sub>5</sub> XANES: Pu(III)aq, Pu(IV)aq, Pu(VI)aq, Pu(IV)col

The preparation procedure described above for the Pu L<sub>3</sub> edge studies is followed also for the M<sub>5</sub> edge studies. Herein we describe only the differences.

- 1) [Pu(III)] and [Pu(IV)] were around 50 mM, whereas [Pu(VI)] around 44 mM;

- The Pu(IV) colloids equilibrated for 9 months were washed with 1 M HClO<sub>4</sub>, and re-suspended in “0.1 M HClO<sub>4</sub>+0.9 M NaClO<sub>4</sub>” (pH = 1);

### TEM

The colloidal Pu(IV) measured with TEM have equilibrated for 9 months. 35 μL of the Pu(IV) colloids were washed with 315 μL of 0.01 M HClO<sub>4</sub>, separated from the solution by 10 kD ultrafiltration and re-suspended in 315 μL 0.01 M HClO<sub>4</sub> (pH 2).

### Pu M<sub>5</sub> HR-XANES: Pu(III)aq and Pu(VI)aq

The preparation procedure described above for the Pu L<sub>3</sub> edge studies is followed also for the M<sub>5</sub> edge studies.

### Pu M<sub>5</sub> HR-XANES: Pu(IV)aq and Pu(IV)col

The preparation procedure described above for the Pu L<sub>3</sub> edge studies is followed also for the M<sub>5</sub> edge studies. Herein we describe only the differences.

- The Vis-NIR analyses for the Pu(IV) aqueous sample showed 94% Pu(IV)<sub>aq</sub> + 6% Pu(VI)<sub>aq</sub> prior the experiment and < 2% increase of Pu(VI) after the Pu M<sub>5</sub> edge experiment; [Pu(IV)] was about 16 mM;
- Due to the small amount of the Pu(IV)col sample, we did not measure the VIS-NIR spectrum after the Pu M<sub>5</sub> HR-XANES but since it was in the same cell as the Pu(IV)aq sample (example of the cell in Figure S6), we do not expect more than 2% variations in the oxidation state; less < 1% Pu(IV)aq and no Pu(VI)aq were detected prior the Pu M<sub>5</sub> HR-XANES experiments (Figure S2).
- The colloidal Pu(IV) species have equilibrated for about 1 year and 10 months; They were separated from the solution by ultrafiltration, washed with 0.5 M HClO<sub>4</sub>, and re-suspended in 200 μL 0.5 M HClO<sub>4</sub>, i.e. pH = 0.3 prior the HR-XANES experiment;

### Vis-NIR spectroscopy

Vis-NIR spectra were measured in semi-micro PMMA cuvettes (Brand) with 1 cm pathlength using a diode array spectrophotometer (Zeiss). Measurements were performed under Argon atmosphere.

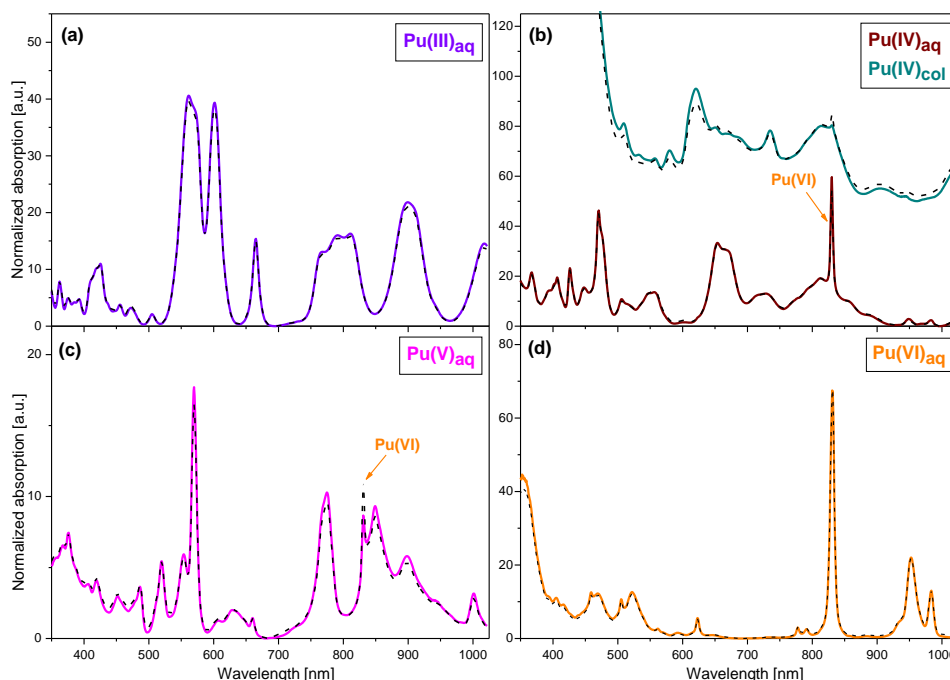


**Fig. S1.** Vis-NIR spectra of Pu(III)<sub>aq</sub> (a), Pu(IV)<sub>aq</sub> (b, bottom), Pu(IV)<sub>col</sub> (b, top), Pu(V)<sub>aq</sub> (c) and Pu(VI)<sub>aq</sub> (d) before (colored curve) and after (black dashed curve) the Pu L<sub>3</sub> edge HR-XANES & XAFS experiments.

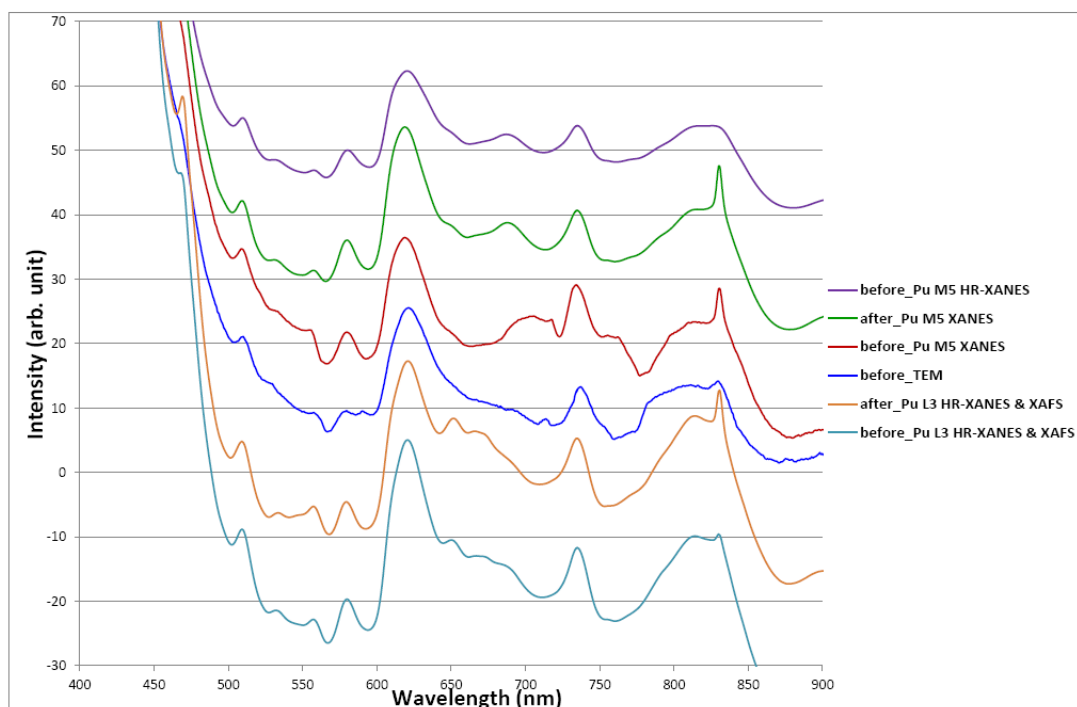


**Fig. S2.** Vis-NIR spectra of Pu(IV)col samples measured before or after HR-XANES/XAFS/TEM experiments (cf. Table S1).

### Transmission electron microscopy (TEM)

Plutonium colloids ca. 0.5  $\mu\text{L}$  (preparation given above) is deposited onto a copper TEM grid with a holey carbon film, corresponding to a total amount of 0.2 nM  $^{242}\text{Pu}$ . High-resolution transmission electron microscopy (HR-TEM), electron energy-loss spectroscopy (EELS), and energy-dispersive X-ray spectroscopy (EDX) were performed using an FEI Tecnai G2 F20 X-TWIN equipment operated at 200 kV. EELS and EDX were performed with a scanning TEM (STEM) mode (STEM-EELS and STEM-EDX).

Figure S4 shows a high resolution -TEM (HR-TEM) image taken from Pu colloids dispersed on the carbon film. The average size of the colloids is less than 5 nm (Figure S3). The inset on the top of Figure S4 depicts a zoom into the area marked by a black rectangle. The crystal lattice fringes with  $d \sim 0.31$  nm and  $d \sim 0.27$  nm are clearly resolved. Based on the assumption that the nano-sized colloids are of  $\text{PuO}_2$  ( $a = 0.5398$  nm, Fm-3m) fluorite type crystal structure, the fringes correspond to ( $d = 0.3117$  nm) and ( $d = 0.2699$  nm) atomic planes, respectively. It was also possible to characterize individual nanocolloids by STEM-EDX and STEM-EELS (see the insets in the bottom of Fig. S4).

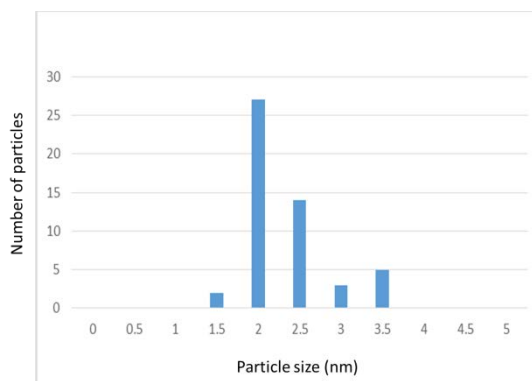


**Fig. S3.** Particle size distribution of colloidal Pu derived from the TEM image (cf. Fig. S4).

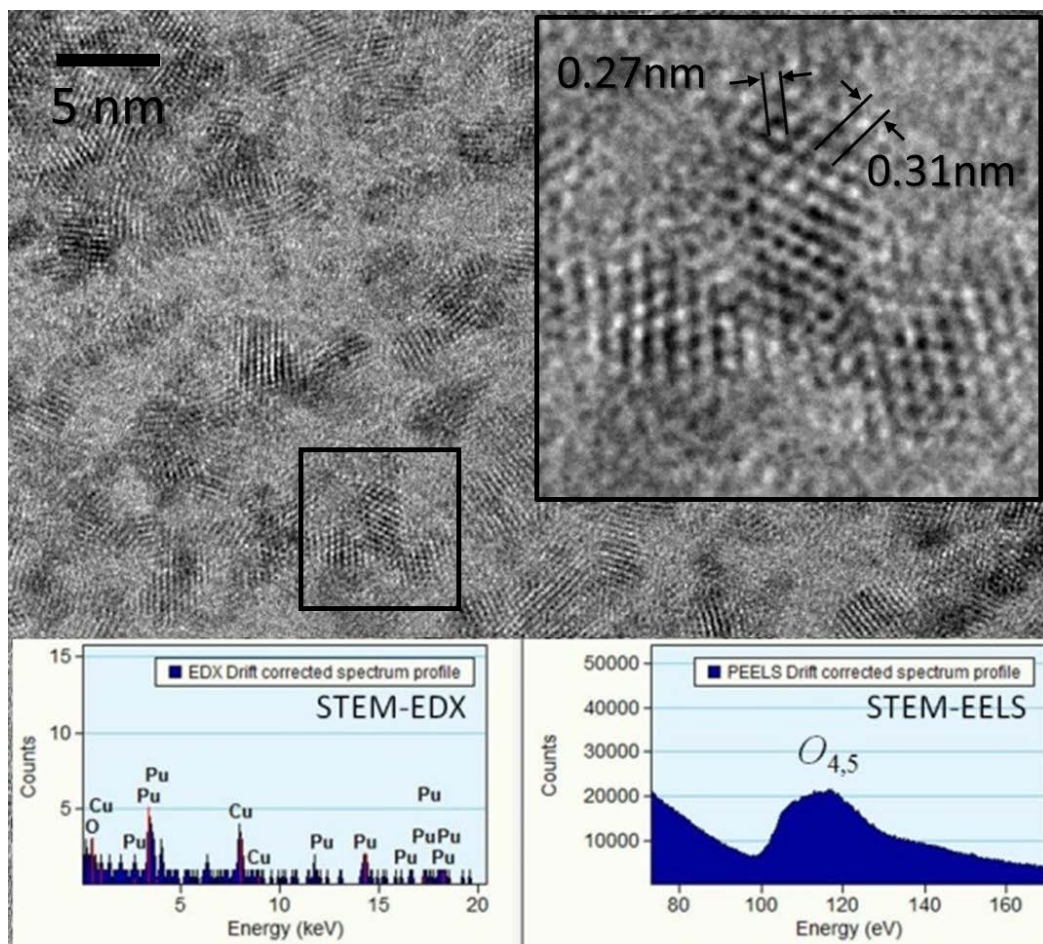


**Fig. S4.** HR-TEM image, STEM-EDX and EELS spectra of nanometer-sized  $\text{PuO}_2$  colloids. The EELS spectrum shows the  $\text{O}_{4,5}$  edge of Pu.

### X-ray absorption spectroscopy

The samples were investigated at the INE-Beamline, Karlsruhe Research Accelerator (KARA) (previous ANKA), Karlsruhe Institute of Technology (KIT), Karlsruhe, Germany. The primary X-ray beam was vertically collimated by a cylindrically bent Rh-coated (INE-Beamline), monochromatized by a Si(111) ( $M_5$ )/Ge(422) ( $L_3$ ) double crystal monochromator (DCM) and focused by a toroidal double focusing Rh coated mirror to an approximate  $0.5 \times 0.5 \text{ mm}^2$  beam spot onto the sample. A detailed description of the INE-Beamline is reported by Rothe et al.<sup>2</sup>

The Pu  $M_5/L_3$  edge HR-XANES spectra were obtained by recording the maximum intensity of the Pu  $M\alpha$  (3351 eV)/ $L\alpha_1$  (14282 eV) emission line diffracted by the five spherically bent Si(220)/Ge(777) crystal analyzers (Saint-Gobain Crystals, France) with 1 m bending radius and focused onto a single diode VITUS Silicon Drift Detector (KETEK, Germany).<sup>3</sup> The crystals were aligned at  $75.22^\circ$  ( $M_5$ )/  $75.7^\circ$  ( $L_3$ ) Bragg angle. The sample, crystals, and detector were arranged in five vertical Rowland circles intersecting at the sample surface and the detector entrance window. No pinhole was used in front of the sample and the crystals were not covered by masks. The experimental energy resolution was estimated for the Pu  $M_5$  edge to be  $1.2 \pm 0.05 \text{ eV}$  by measuring the full width at half maximum (fwhm) of the incident beam elastically scattered from a Teflon sample. It was not possible to measure it for the  $L_3$  edge since the intensity of the elastic peak was too low.

For the An  $L_3$  HR-XANES/XAFS experiments the aqueous and colloidal solutions were placed in 300  $\mu\text{l}$  vials and positioned in the inert gas cell shown in Fig. S5 (top). Ar gas was flushed continuously during the experiment.

For the An  $M_5$  XANES/HR-XANES experiments the liquid cells depicted in Fig. S5 were used; about 200  $\mu\text{l}$  sample was filled in each cell; 10 and 13  $\mu\text{m}$  thick Kapton films were used as first and second window, respectively. He gas was flushed continuously during the experiment.

The averaged Pu  $M_5$  and  $L_3$  edge XANES/HR-XANES spectra were normalized by subtraction of a linear background function from the featureless pre-edge region and normalization of the edge jump to unity. The energy positions of the main absorption peaks (WLs) reported in the publication are the energy positions of the zero crossings of the first derivatives of the spectra. The energy positions of the maximum intensity of the multiple scattering peaks (B in Fig. 1 in the manuscript and C in Fig. S9) of the Pu  $L_3$  HR-XANES spectra for Pu(V)-yl and Pu(VI)-yl are estimated.

### Pu $M_5$ XANES and HR-XANES

The DCMs was calibrated by assigning 3775 eV to the maximum of the most intense absorption resonance (white line, WL) of the Pu  $M_5$  edge HR-XANES spectrum of a PuO<sub>2</sub> reference sample. The energy calibration of the DCM has  $\pm 0.05$  eV uncertainty equal to half of the energy step size. A gastight box enclosing the spectrometer and the sample maintaining constant He atmosphere (ambient pressure) during all measurements was installed to avoid intensity losses due to scattering and absorption of photons in the tender X-ray regime. A Pu  $M_5$  edge HR-XANES spectrum and a normal emission line for the PuO<sub>2</sub> reference were measured after each Pu sample to verify the calibration of the DCM and the alignment of the spectrometer. The Pu  $M_5$  XANES spectra were measured in fluorescence mode using a single diode VITUS Silicon Drift Detector (KETEK, Germany). Pu  $M_5$  XANES/HR-XANES spectra were recorded from 3760 to 3835 eV with varying step sizes 3760–3770 eV: 0.5 eV; 3770–3790 eV: 0.1 eV; 3790–3835 eV: 0.5 eV (e.g. 1 s/step for the XANES/HR-XANES spectrum of Pu(VI)aq). Typically, two to three scans were collected at room temperature and averaged.

### Pu $L_3$ HR-XANES & XAFS

Pu  $L_3$  edge X-ray absorption fine structure (XAFS = XANES + EXAFS) spectra were recorded simultaneously in fluorescence and transmission detection mode; only the latter EXAFS spectra were modeled and the XANES spectra are shown in Fig. 1. In fluorescence mode the intensity of the Pu  $L\alpha_1$  (14282 eV) fluorescence line was measured using a five-element high purity Ge-solid state (Canberra). Zr (K edge = 17 998 eV) foil was simultaneously measured with all samples (HR-XANES and XAFS) to control the energy calibration of the DCM. The energy calibration of the DCM has  $\pm 0.25$ eV uncertainty equal to half of the energy step size in the XANES region. Three to six scans were collected at room temperature and averaged for each sample in the range of 17 877–19 306 eV; a 0.5 eV step size was used in the XANES region of the spectra, and equidistant k steps (0.04  $\text{\AA}^{-1}$ ) were used in the post edge EXAFS region.

The EXAFS spectra ( $\chi(k)$ ) were extracted, Fourier transformed, and modeled using the ATHENA and ARTEMIS programs included in the IFEFFIT program package.<sup>4</sup> The spectra were weighted by  $k = 1, 2,$  and  $3$  within  $k$  range  $2.7$ - $9.5 \text{ \AA}^{-1}$ . The single and multiple scattering paths used to model the experimental spectra were calculated by the FEFF8.2 code.<sup>5</sup> A shell by shell approach was applied to model the data in R space within a range of R from  $1.05 \text{ \AA}$  to  $3.7 \text{ \AA}$  for Pu(IV)<sub>col</sub> and from  $R = 1.05 \text{ \AA}$  to  $2.55 \text{ \AA}$  for the aqueous Pu species. The amplitude reduction factor was set to 1 and was fixed during the fitting process.

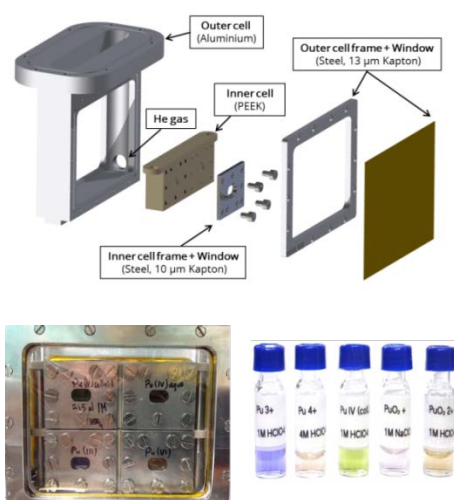


**Fig. S5.** 3d view of the inert gas cell used for the  $L_3$  and  $M_5$  edge experiments (top); 3d view (top) and a photograph (bottom) of the liquid cells used for the  $M_5$  edge experiments. A photograph of the aqueous and colloidal Pu samples prepared for the Pu  $L_3$  edge HR-XANES/XAFS experiments (bottom right).

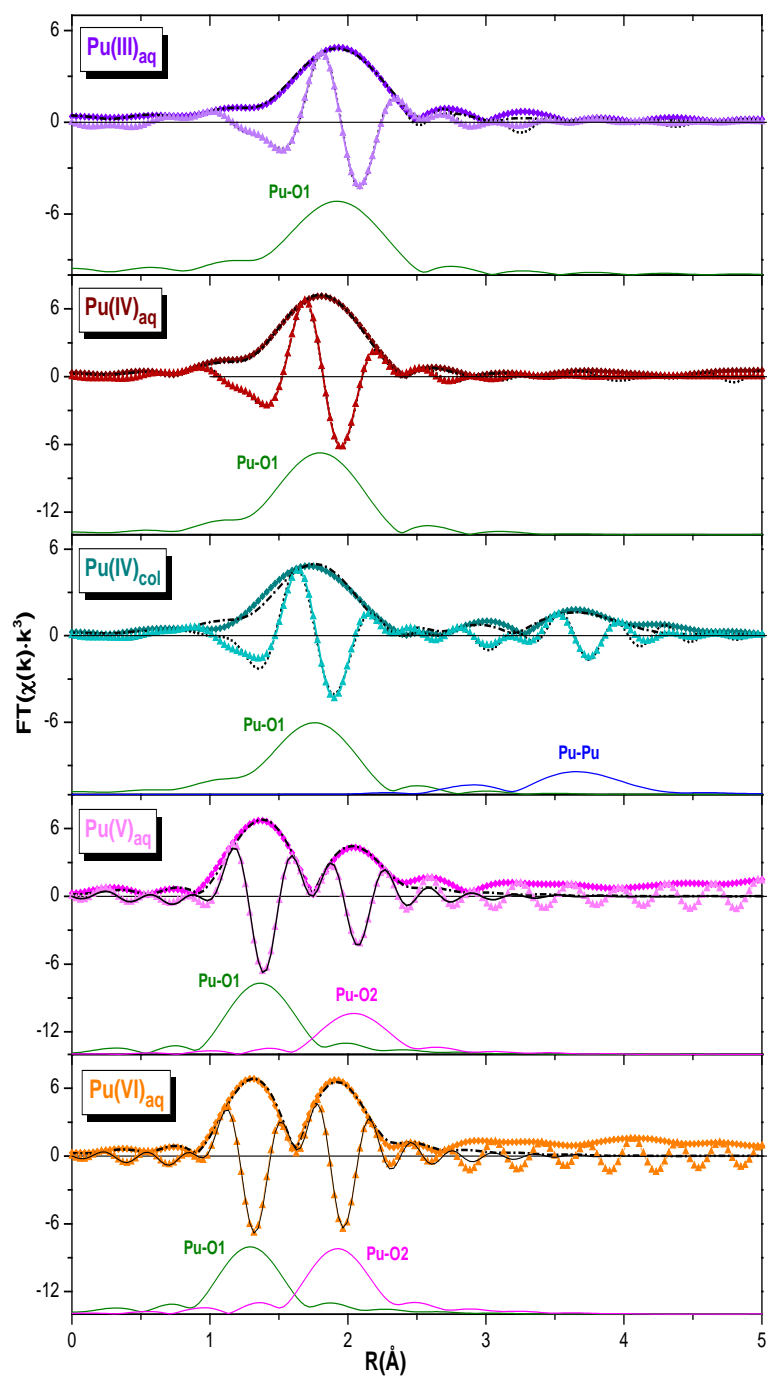


**Fig. S6.** Magnitude of Fourier transformed EXAFS spectra (coloured rhombs) and their best fits (dash dot line) for Pu(III)<sub>aq</sub>, Pu(IV)<sub>aq</sub>, Pu(IV)<sub>col</sub>, Pu(V)<sub>aq</sub> and Pu(VI)<sub>aq</sub>. The arrow indicates Pu-Pu coordination peak in Pu(IV)<sub>col</sub>.

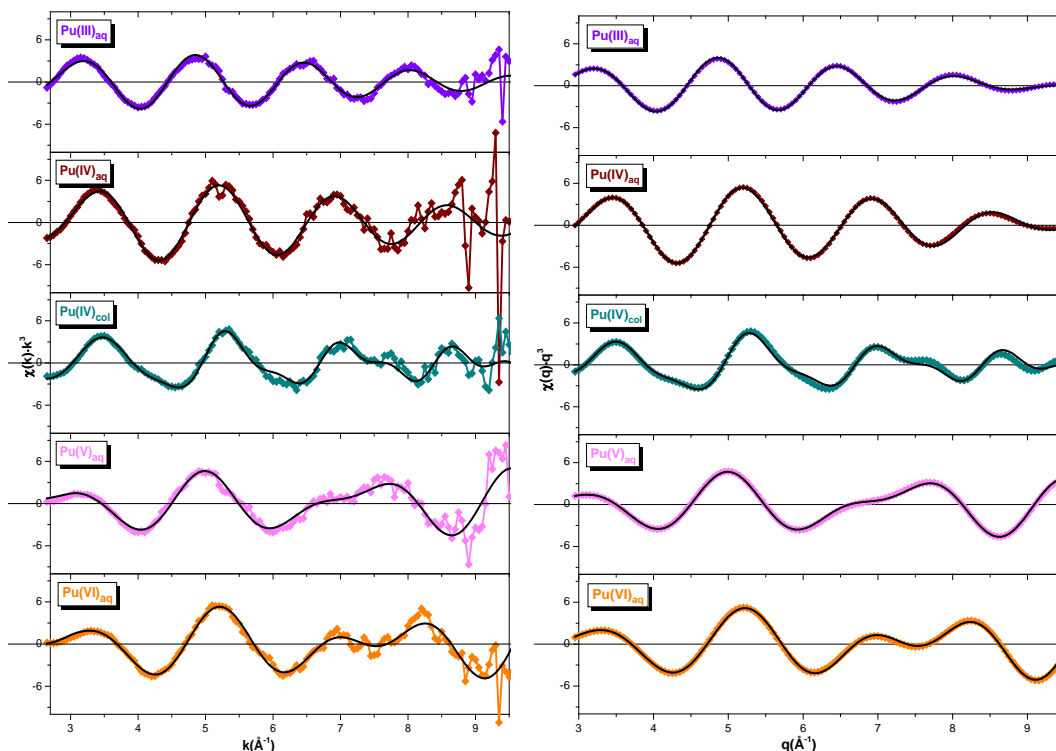


**Fig. S7.** EXAFS spectra in  $k$  and back transformed  $q$  range and their best fits for the  $\text{Pu(III)}_{\text{aq}}$ ,  $\text{Pu(IV)}_{\text{aq}}$ ,  $\text{Pu(IV)}_{\text{col}}$ ,  $\text{Pu(V)}_{\text{aq}}$  and  $\text{Pu(VI)}_{\text{aq}}$ .

**Table S2.** EXAFS fit results: SP – scattering path, N – coordination number, R – bond distance,  $\sigma^2$  – Debye-Waller factor,  $\Delta E_0$  – energy shift of the ionization potential,  $S_0^2$  – amplitude reduction factor and  $r$  – goodness of fit parameter.  $N^*$  and  $R^*$  – coordination numbers and average interatomic distances derived from optimized structures with TURBOMOLE ( $\text{Pu(IV)}_{\text{aq}}$ ,  $\text{Pu(V)}_{\text{aq}}$ ,  $\text{Pu(VI)}_{\text{aq}}$ ) or  $\text{PuO}_2$  ICSD 55456 ( $\text{Pu(IV)}_{\text{col}}$ );\*\* Published coordination number and interatomic distances.<sup>6</sup>

Sample	SP	N	$N^*$	$N^{**}$	R [Å]	$R^*$ [Å]	$R^* - R$	$R^{**}$ [Å]	$\Delta E_0$ [eV]	$\sigma^2 \cdot 10^{-3}$ [Å <sup>2</sup> ]	$S_0^2$	$r$
$\text{Pu(III)}_{\text{aq}}$	Pu-O1	10.5(8)	9	8-9	2.48(1)	2.568	0.088	2.49(1)	-3.2(8)	10(2)	1.0	0.001
$\text{Pu(IV)}_{\text{aq}}$	Pu-O1	11.2(5)	9	8-9	2.34(1)	2.477	0.137	2.39(1)	-4.4(5)	10(1)	1.0	0.001
$\text{Pu(IV)}_{\text{col}}$	Pu-O1	7.9(1)	8		2.30(1)	2.338	0.038		4.2(8)	10(1)	1.0	0.006
	Pu-Pu	6.2(9)	12		3.78(2)	3.817	0.037					
$\text{Pu(V)}_{\text{aq}}$	Pu-O1	2.0(4)	2	2	1.82(1)	1.738	-0.082	1.81(1)	5.2(7)	3(2)	1.0	0.005
	Pu-O2	2.7(3)	5	4-5	2.50(1)	2.467	-0.033	2.47(1)				
$\text{Pu(VI)}_{\text{aq}}$	Pu-O1	1.7(2)	2	2	1.74(1)	1.784	0.044	1.75(1)	2.5(9)	0.6(5)	1.0	0.002
	Pu-O2	3.7(4)	5	4-5	2.39(1)	2.575	0.185	2.41(1)				

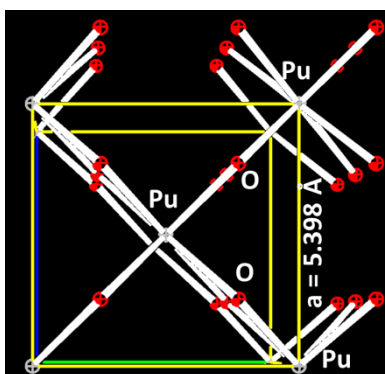


**Fig. S8.** The unit cell of PuO<sub>2</sub> (ICSD 55456), The lattice constant  $a = 5.398 \text{ \AA}$  is given.

### Modeling of the Pu L<sub>3</sub> HR-XANES spectrum of Pu(VI)aq

Linear combination least-squares (LCLS) fit analyses of the Pu L<sub>3</sub> HR-XANES spectrum of Pu(VI)aq was performed with the WINXAS program ([www.winxas.de](http://www.winxas.de)) using three pseudo-Voigt (PV) [ $f(x) = \alpha \text{Gaussian} + (1 - \alpha) \text{Lorentzian}$ ] and one arctangent functions. The Levenberg–Marquardt least-squares algorithm is used in the fit. The results are depicted in Fig. S7 and Table S4.

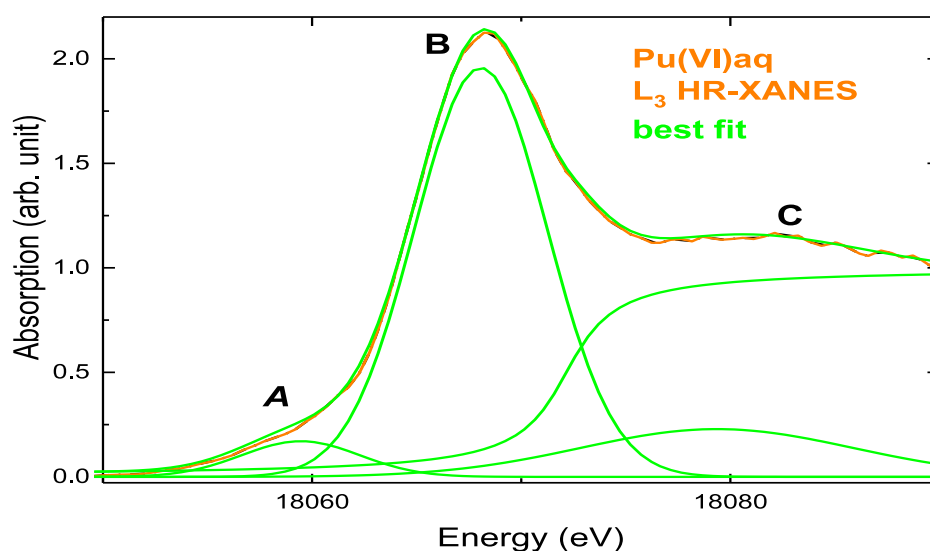


**Fig. S9.** The experimental Pu L<sub>3</sub> HR-XANES spectrum for Pu(VI)aq modeled with three Voigt profiles and one arctan function.

**Table S3.** Spectral feature, Height, Position and Full width at half maximum (FWHM) parameters of the PV functions used to model the Pu L<sub>3</sub> HR-XANES spectrum and an arctangent used to model the edge jump; the Gauss part (Gauss part  $\alpha$ ) and the area of the PV profiles (Area PV); the residual between experimental data and best fit (Residual %); <sup>f</sup> denotes that the parameter is fixed during the fit.

Spectral Feature	Height $\pm 0.01$	Position $\pm 0.1$ eV	FWHM $\pm 0.1$ eV	Gauss part $\alpha$	Area of PV	Residual %
A	0.17	18059.5	6.7	1	1.2	2
B	1.96	18068.1	7.5	1	15.6	2
C	0.23	18079.4	15.3	1	3.7	2
arctan	1 <sup>f</sup>	18072.2	5.5		23.9	2

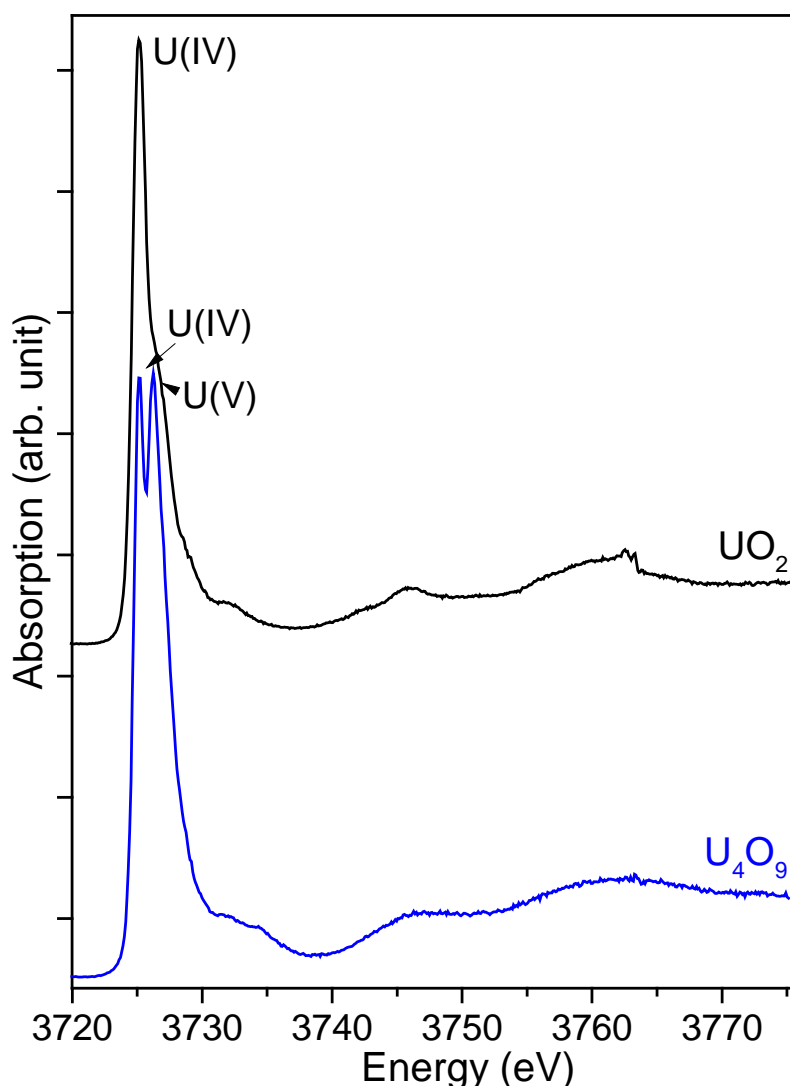


**Fig. S10.** U M<sub>4</sub> HR-XANES spectra of UO<sub>2</sub> and U<sub>4</sub>O<sub>9</sub> reported in references 1 and 7. The data is reproduced from *Phys Rev Lett* 2013, **111**, 253002 (Ref. 7) with permission of the authors.

### Quantum chemical calculations

*Ab-initio* quantum chemical calculations of Pu L<sub>3</sub> edge HR-XANES spectra and Pu, O density of states (DOS) were performed with the FEFF9.5 code based on the multiple scattering theory.<sup>8,9</sup> The most important cards used in the FEFF9.5 calculations are listed in Table S4 (cf. feff.inp examples below). The potentials of free atoms were calculated with a relativistic Dirac–Fock atom code part of FEFF9.5. The scattering potentials were calculated self-consistently by overlapping the free atomic density in the muffin thin approximation within a cluster of 8/10 ((Pu)aq)/238 (Pu(IV)col) atoms (SCF card). The UNFREEZE card was used to include the Pu f states in the SCF calculation providing their accurate energy position and shape.<sup>10</sup> The energy dependent exchange Hedin–Lundquist potential was used for the fine structure and the atomic background (EXCHANGE card). Dipole or dipole + quadrupole (dip+quad) transitions are considered (MULTIPOLE card). The core-hole lifetime broadening was reduced by 2.5 eV leading to a broadening of 6.2 eV.<sup>10</sup> No experimental broadening was considered. The full multiple scattering XANES spectra were calculated for an atomic cluster of 8/10/238 atoms centered on the absorbing Pu atom (FMS and XANES cards). Best agreement between calculation and experiment was found by applying the default option to screen the 2p<sub>5/2</sub> core-hole (COREHOLE FSR). The TURBOMOLE package<sup>11,12</sup> (DFT/BP86 with TZVP basis sets) was applied to optimize the structures of the

aqueous Pu species used in the calculations; H atoms were omitted; PuO<sub>2</sub> crystal structure (ICSD 55456) was utilized for the colloidal Pu(IV).

**Table S4.** Input parameters used in the feff.inp files.

Pu species	SCF <sup>a</sup>	EXCHANGE <sup>b</sup>	UNFREEZE <sup>c</sup>	EGRID <sup>d</sup>	MULTIPOLE <sup>e</sup>	Number of atoms <sup>f</sup>
Pu(III) <sub>aq</sub>	5.0 1 100 0.05 6	0 0 -2.5	yes	-15 0 0.2	dip/dip+quad	10
Pu(IV) <sub>aq</sub>	5.0 1 100 0.05 6	0 0 -2.5	yes	-15 0 0.2	dip/dip+quad	10
Pu(IV) <sub>col</sub>	5.0 1 100 0.05 6	0 0 -2.5	yes	-15 0 0.2	dip/dip+quad	238
Pu(V) <sub>aq</sub>	5.0 1 100 0.05 6	0 0 -2.5	Yes	-15 0 0.2	dip/dip+quad	8
Pu(VI) <sub>aq</sub>	5.0 1 100 0.05 6	0 0 -2.5	Yes	-15 0 0.2	dip/dip+quad	8

<sup>a</sup> Self-consistent field (SCF) card: the scattering potentials are calculated self-consistently;

<sup>b</sup> Specifies the energy dependent exchange correlation potential; the third parameter sets 2.5 eV reduction of core-hole lifetime broadening;

<sup>c</sup> When it is not used the f electron density is fixed at the atomic value;

<sup>d</sup> used to customize the energy grid;

<sup>e</sup> It is used to define if only dipole or dipole and quadrupole transitions are considered;

<sup>f</sup> Number of atoms used in the calculation;

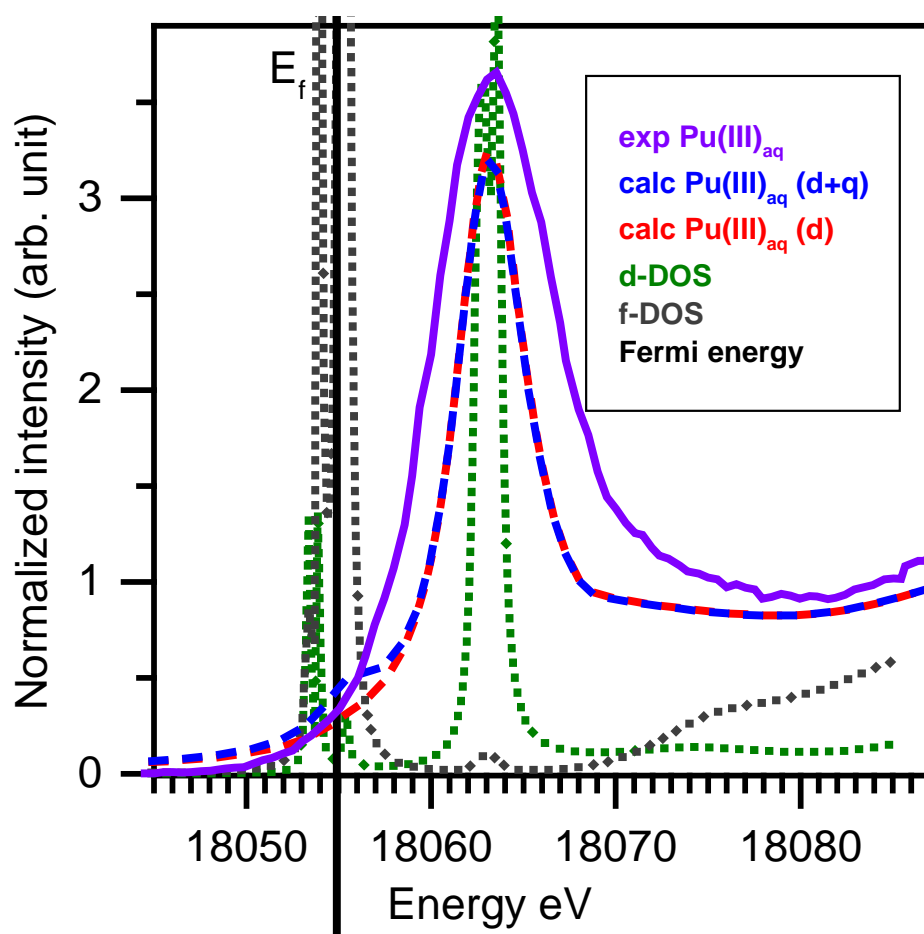


**Fig. S11.** Pu L<sub>3</sub> HR-XANES: experiment and calculations with the FEFF9.5 code and Pu d- and f-DOS for Pu(III)<sub>aq</sub>.

**Example of a feff.inp file for calculation of Pu L<sub>3</sub> HR-XANES and DOS for Pu(III)aq**

```
* Pu L3 PuIII 9H2O
EDGE L3
S02 1.0

* pot xsph fms paths genfmt ff2chi
CONTROL 1 1 1 1 1 1
PRINT 1 0 0 0 0 0

EXCHANGE 0 0 -2.5

SCF 5.0 1 100 0.05 6

EGRID
e_grid -15 0 0.2
k_grid last 5 0.05

XANES 4.0
FMS 5 1

MULTIPOLE 2
UNFREEZE
LDOS -30 20 0.1

POTENTIALS
* ipot Z element l_scmt l_fms stoichiometry
  0 94 Pu -1 -1
  1 8 O -1 -1

ATOMS
0.000000 0.000000 0.000000 0 Pu
-1.2819068 -2.2203276 0.000000 1 O
-1.2819068 2.2203276 0.000000 1 O
2.5638135 0.000000 0.000000 1 O
0.8671266 -1.5613353 -1.8484935 1 O
0.9185928 -1.5316213 1.8484935 1 O
0.9185928 1.5316213 -1.8484935 1 O
0.8671266 1.5613353 1.8484935 1 O
-1.7857194 0.0297140 -1.8484935 1 O
-1.7857194 -0.0297140 1.8484935 1 O
```

**Example of a feff.inp file for calculation of Pu L<sub>3</sub> HR-XANES and DOS for Pu(IV)col**

```
TITLE Pu O2

EDGE L3
S02 1.0

* pot xsph fms paths genfmt ff2chi
CONTROL 1 1 1 1 1 1
PRINT 1 0 0 0 0 0

EXCHANGE 0 0 -2.5

SCF 5.0 0 100 0.05 6
```

EGRID  
e\_grid -15 0 0.2  
k\_grid last 5 0.05

XANES 4.0  
FMS 8 0

\* MULTIPOLE 2  
UNFREEZE F  
LDOS -30 20 0.1

POTENTIALS  
0 94 Pu 3 3 0.0010  
1 94 Pu 3 3 4.0  
2 8 O 1 1 8.0

ATOMS

0.00000	0.00000	0.00000	0 Pu1	0.00000	0
1.34375	1.34375	1.34375	2 O1	2.32744	1
-1.34375	1.34375	1.34375	2 O1	2.32744	2
1.34375	-1.34375	1.34375	2 O1	2.32744	3
-1.34375	-1.34375	1.34375	2 O1	2.32744	4
1.34375	1.34375	-1.34375	2 O1	2.32744	5
-1.34375	1.34375	-1.34375	2 O1	2.32744	6
1.34375	-1.34375	-1.34375	2 O1	2.32744	7
-1.34375	-1.34375	-1.34375	2 O1	2.32744	8
2.68750	2.68750	0.00000	1 Pu1	3.80070	9
-2.68750	2.68750	0.00000	1 Pu1	3.80070	10
2.68750	-2.68750	0.00000	1 Pu1	3.80070	11
-2.68750	-2.68750	0.00000	1 Pu1	3.80070	12
2.68750	0.00000	2.68750	1 Pu1	3.80070	13
-2.68750	0.00000	2.68750	1 Pu1	3.80070	14
0.00000	2.68750	2.68750	1 Pu1	3.80070	15
0.00000	-2.68750	2.68750	1 Pu1	3.80070	16
2.68750	0.00000	-2.68750	1 Pu1	3.80070	17

The list with atoms continues to 238 atoms

- (1) Pidchenko, I.; Kvashnina, K. O.; Yokosawa, T.; Finck, N.; Bahl, S.; Schild, D.; Polly, R.; Bohnert, E.; Rossberg, A.; Gottlicher, J.; Dardenne, K.; Rothe, J.; Schafer, T.; Geckeis, H.; Vitova, T. *Environ Sci Technol* **2017**, *51*, 2217.
- (2) Rothe, J.; Butorin, S.; Dardenne, K.; Denecke, M. A.; Kienzler, B.; Loble, M.; Metz, V.; Seibert, A.; Steppert, M.; Vitova, T.; Walther, C.; Geckeis, H. *Rev Sci Instrum* **2012**, *83*.
- (3) Zimina, A.; Dardenne, K.; Denecke, M. A.; Doronkin, D. E.; Huttel, E.; Lichtenberg, H.; Mangold, S.; Pruessmann, T.; Rothe, J.; Spangenberg, T.; Steininger, R.; Vitova, T.; Geckeis, H.; Grunwaldt, J. D. *Rev Sci Instrum* **2017**, *88*.
- (4) Ravel, B.; Newville, M. *J Synchrotron Radiat* **2005**, *12*, 537.
- (5) Ankudinov, A. L.; Ravel, B.; Rehr, J. J.; Conradson, S. D. *Phys Rev B* **1998**, *58*, 7565.
- (6) Conradson, S. D.; Abney, K. D.; Begg, B. D.; Brady, E. D.; Clark, D. L.; den Auwer, C.; Ding, M.; Dorhout, P. K.; Espinosa-Faller, F. J.; Gordon, P. L.; Haire, R. G.; Hess, N. J.; Hess, R. F.; Keogh, D. W.; Lander, G. H.; Lupinetti, A. J.; Morales, L. A.; Neu, M. P.; Palmer, P. D.; Paviet-Hartmann, P.; Reilly, S. D.; Runde, W. H.; Tait, C. D.; Veirs, D. K.; Wastin, F. *Inorg Chem* **2004**, *43*, 116.
- (7) Kvashnina, K. O.; Butorin, S. M.; Martin, P.; Glatzel, P. *Phys Rev Lett* **2013**, *111*, 253002.
- (8) Rehr, J. J.; Kas, J. J.; Prange, M. P.; Sorini, A. P.; Takimoto, Y.; Vila, F. *Cr Phys* **2009**, *10*, 548.
- (9) Rehr, J. J.; Kas, J. J.; Vila, F. D.; Prange, M. P.; Jorissen, K. *Phys Chem Chem Phys* **2010**, *12*, 5503.

- (10) Vitova, T.; Green, J. C.; Denning, R. G.; Löble, M.; Kvashnina, K.; Kas, J. J.; Jorissen, K.; Rehr, J. J.; Malcherek, T.; Denecke, M. A. *Inorganic Chemistry* **2015**, *54*, 174.
- (11) TURBOMOLE GmbH 2016 ed. University of Karlsruhe and Forschungszentrum Karlsruhe, 1989-2007.
- (12) Furche, F.; Ahlrichs, R.; Hattig, C.; Klopper, W.; Sierka, M.; Weigend, F. *Wiley Interdisciplinary Reviews-Computational Molecular Science* **2014**, *4*, 91.